

MULTI-SCALE DESCRIPTION OF PEDESTRIAN COLLECTIVE DYNAMICS WITH PORT-HAMILTONIAN SYSTEMS*

ANTOINE TORDEUX

School of Mechanical Engineering and Safety Engineering
University of Wuppertal
Wuppertal, Germany

CLAUDIA TOTZECK

School of Mathematics and Natural Sciences
University of Wuppertal
Wuppertal, Germany

(Communicated by the associate editor name)

ABSTRACT. Port-Hamiltonian systems (PHS) theory is a recent but already well-established modelling approach for non-linear physical systems. Some studies have shown lately that PHS frameworks are relevant for modelling and control of swarm and multi-agent systems. We identify in this contribution a general class of microscopic force-based pedestrian models that can be formulated as a port-Hamiltonian system. The pedestrian PHS has linear structure and dissipation components. Non-linear effects come from isotropic pedestrian interactions. Simulation results on a torus with disordered initial states show that the port-Hamiltonian pedestrian model can exhibit different types of dynamics. They range from relaxed speed models with no interaction, dynamical billiards, or crystallization dynamics to realistic pedestrian collective behaviors, including lane and strip formation for counter and crossing flow. The port-Hamiltonian framework is a natural multiscale description of pedestrian dynamics as the Hamiltonian turns out to be a generic order parameter that allows us to identify specific behaviours of the dynamics from a macroscopic viewpoint. Particular cases even enable through energy balance to determine the Hamiltonian behavior without requiring the tedious computation of the microscopic dynamics. Using PHS theory, we systematically identify a critical threshold value for the Hamiltonian, which relies only on exogenous input and can be physically interpreted.

1. Introduction. Port-Hamiltonian systems (PHS) are recent modelling approaches for nonlinear physical systems [2, 3]. They date back to the 1980s and the pioneer works of Arjan van der Schaft and Bernhard Maschke on Hamiltonian systems with inputs and outputs [4, 5]. The modelling concept, initially called *Port-Controlled Hamiltonian Systems*, was established during the 1990s [6]. The terminology *Port-Hamiltonian Systems* was democratized during the 2000s [2, 3] and is nowadays increasingly predominant (see Fig. 1). While Hamiltonian systems are often referred to as conservative systems, PHS enable for dissipation and their ports can be

2020 *Mathematics Subject Classification.* Primary: 76A30, 34C60; Secondary: 82C22.

Key words and phrases. Pedestrian dynamics, force-based model, port-Hamiltonian system, collective dynamics, Hamiltonian order parameter, multiscale description.

The first author is supported by NSF grant xx-xxxx.

*Corresponding author: First-name1 last-name1.

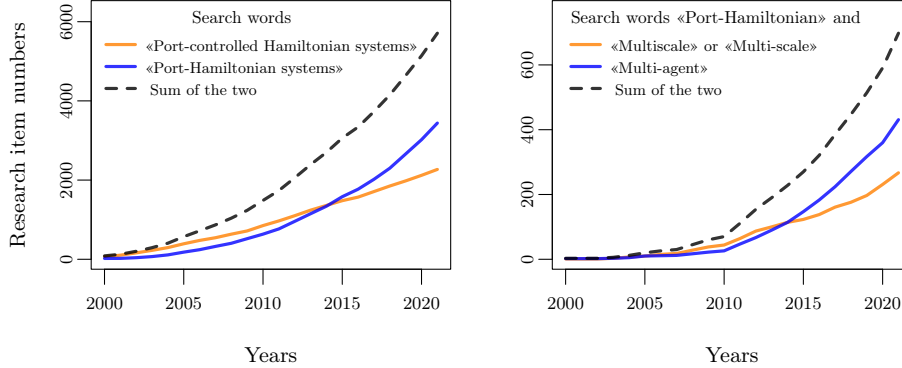


FIGURE 1. Cumulative research item numbers from 2000 to 2021 for the search words «Port-controlled Hamiltonian systems» and «Port-Hamiltonian systems» (left plot) and the search words «Port-Hamiltonian» and «Multi-agent» or «Multiscale» (right plot). Requests done on googlescholar [1] the 22.08.2022.

used for control actions and external factors influencing the dynamics. The modelling approach also allows for straightforward computation of the system output and Hamiltonian behavior.

To fix the setting and some standard PHS terms we recall the structure of a PHS system with Hamiltonian $H: \mathbb{R}^n \rightarrow \mathbb{R}$ as follows:

$$\dot{z}(t) = (J - R)\nabla H(z(t)) + Bu(t), \quad y(t) = B^\top \nabla H(z(t)),$$

where $J \in \mathbb{R}^{n \times n}$ is skew-symmetric, $R \in \mathbb{R}^{n \times n}$ positive semi-definite, $B \in \mathbb{R}^{n \times m}$ with *state* z and *output* y . In most of the examples the input $u(t) \in \mathbb{R}^m$ is lower dimensional than the state, i.e. $m \ll n$. For $B \equiv 0$ and $R \equiv 0$ we obtain a conservative Hamiltonian system. $R > 0$ yields *dissipation* and the input u allows to feed energy into the dynamics. This can be understood mathematically with a simple calculation. Indeed, with the skew-symmetry of J and the positive semi-definiteness of R , it holds

$$\begin{aligned} \dot{H}(z(t)) &= \nabla H(z(t)) \cdot \dot{z}(t) \\ &= \nabla H(z(t)) \cdot ((J - R)\nabla H(z(t)) + Bu(t)) \\ &= -\nabla H(z) \cdot R\nabla H(z(t)) + \nabla H(z(t)) \cdot Bu(t) \\ &\leq y(t) \cdot u(t) \end{aligned}$$

In the classical Hamiltonian framework the skew-symmetry yields a zero right-hand side with means the system is conservative. For $R > 0$ we obtain an inequality which accounts for the dissipation. $u \neq 0$ allows to feed in or pull out energy, making the system *reactive*. As the input and output allows for coupling of PH systems and to exchange information, they are denoted *ports*.

PHS were initially designed for network and graph modelling [7, 8]. Nowadays, various physical domains, including thermodynamics, electromechanics, electromagnetics, fluid mechanics, or hydrodynamics, can be tackled using PHS (see the review [9]). Indeed, the PHS functional structure, mitigating the modelling between conserved quantities, dissipation, input and output, is a meaningful representation of

many systems. Recent results have shown the relevance of PHS for self-propelled multi-agent systems modelling and control [10]. Such a recent expansion partly comes from the analogy between multi-agent systems and (dynamic) graphs [11]. Examples of port-Hamiltonian multi-agent systems arise in reliability engineering, for complex mechanical systems [12, 13], consensus and opinion formation [14, 15], multi-input multi-output multi-agent systems [16], swarm behaviors [17], or autonomous vehicles, e.g., path-tracking [18] or modelling and safety analysis of adaptive cruise control systems [19, 20, 21]. Such microscopic agent-based modelling approaches rely on PHS by ordinary, stochastic, or delayed differential equation systems. At macroscopic scales, traffic flow models [22] and fluid dynamics models [23] are based on infinite-dimensional PHS by partial differential equations using Stokes-Dirac structures as bond graph representations. In all the modelling approaches, the Hamiltonian quantifies a (generalized) total energy of the system.

Besides structural advantages and preservation of physical quantities, technical benefits of PHS yield well-posedness and uniqueness properties of the solutions, energy balance, and a well-established stability analysis using the Hamiltonian as Lyapunov function [2, 3].

Classical pedestrian models rely on three behavior levels. At the strategic level, pedestrians decide on their activity and associated travel needs. The tactical level concerns short-term decisions, e.g., choosing the route by considering obstacles and local pedestrian densities. The operational level describes the pedestrian motion resulting from interaction with immediate surroundings, for example, collision avoidance while maintaining a steady course. The processes at strategic and tactical level are usually considered as exogenous control factors in operational pedestrian simulations.

Operational pedestrian models exist since the 1970s and were introduced in the pioneering works by Hirai and Tarui on microscopic simulations [24] and by Henderson on macroscopic crowd representation [25]. Nowadays, the modelling approaches range from macroscopic, mesoscopic, and microscopic models, among other modeling scale characteristics [26, 27]. Macroscopic and mesoscopic approaches come from continuous fluid dynamics or gas-kinetic models describing aggregated flow behaviors in Eulerian domains, while microscopic approaches reproduce individual pedestrian motions in Lagrangian frameworks. Many reviews focus on pedestrian modeling scales and passages from one modeling level to another [28, 29, 30]. Indeed, mesoscopic or macroscopic representations are in practice easier to analyse than multi-agent microscopic systems. Hydrodynamic and mean-field limits are some of the most used techniques [29, 31, 32, 33, 34]. Numerous studies rely on individual pedestrian motions with microscopic continuous approaches, notably with the social force model (SFM) [35]. The social force model is an inertial, second-order operational approach belonging to the force-based model class [36]. Speed-based models inspired by robotics, e.g., the reciprocal velocity avoidance (RVO) and optimal, reciprocal collision avoidance (ORCA) first-order models [37, 38], are also relevant in the field, notably for computer graphics animation [39]. One of the advantages of microscopic approaches compared to macroscopic ones is their natural ability to reproduce heterogeneous behaviors and notably mixed flow of pedestrians with different desired directions. The challenge consists of identifying microscopic underlying mechanisms and interaction types initiating the emergence of collective

phenomena such as lane and strip formation for counter and crossing flow, respectively. The emergence of collective dynamics can be detected by stability analysis [29, 32, 40] or with the help of order parameters [41, 42].

In this contribution, we identify a generic class of force-based pedestrian models that can be formulated as a port-Hamiltonian system by a second-order ordinary differential equation system. In contrast, to the modelling approach has been proposed recently for the Cucker-Smale swarm model [17], the dynamics here is not only self-propelled but allows for desired velocities or paths of the pedestrians. PHS is found to be a pertinent modelling framework for pedestrian behaviors by decomposing the dynamics between interaction, dissipation, and control, i.e., input and output. A modelling parallel between force-based pedestrian models and the port-Hamiltonian formulation is discussed. Besides explicit control of the dynamics through the agents' input ports, the PHS formulation has the advantage of a direct multiscale framework since the aggregated information of the Hamiltonian can be used to define a macroscopic order parameter. In the literature, the order parameters are generally tailored to identify specific collective dynamics. Here, the systematic quantification of system energy through the Hamiltonian offers a generic order parameter to analyse pedestrian collective dynamics. In particular cases, energy balance allows determining the Hamiltonian behaviour without requiring the tedious computation of the microscopic dynamics. This makes port-Hamiltonian systems a promising modelling approach for pedestrian dynamics that we aim to explore further.

The manuscript is organised as follows: we present the microscopic force-based pedestrian model, its port-Hamiltonian formulation, and appropriate numerical discretization schemes in the next section. Simulation results on a torus with disordered initial states show that the port-Hamiltonian pedestrian model can describe different types of dynamics in Sec. 3.2. We first analyse specific cases for which repulsive interaction, dissipation, or input are zero to illustrate the role of the different model components on the dynamics. Collective pedestrian dynamics, including lane and strip formation for counter and crossing flow, and their characterisation using an order parameter based on the Hamiltonian are shown hereafter. Sec. 5 provides a conclusion and further perspectives for port-Hamiltonian pedestrian modelling.

2. Port-Hamiltonian pedestrian model. We begin with the presentation of the details of the microscopic pedestrian model. Then the dynamics is rewritten to show its port-Hamiltonian structure. The section concludes with a discussion of different scenarios for the evolution of the Hamiltonian over time.

2.1. Microscopic dynamics. We consider $N \geq 2$ particles on a torus with position

$$q_i: [0, T] \rightarrow \mathbb{R}^2$$

and momentum

$$p_i: [0, T] \rightarrow \mathbb{R}^2$$

for $i = 1, \dots, N$. By

$$Q_{ij}(t) = q_i(t) - q_j(t) \in \mathbb{R}^2,$$

we denote the relative position of pedestrian i to pedestrian j at time $t \in [0, T]$. For notational convenience, we collect the relative positions of pedestrian i in the vector,

$$Q_i = (Q_{ij})_{j \neq i}: [0, T] \rightarrow \mathbb{R}^{2 \cdot (N-1)} \text{ for } i, j = 1, \dots, N, j \neq i.$$

Throughout the article, we assume that the pedestrians have normalized mass, i.e. $m = 1$, hence momentum and velocity coincide. Following the classical modelling approach of force-based models [27, 35, 36], we identify two main components in operational pedestrian dynamics:

1. isotropic short-range repulsion among neighboring pedestrians;
2. relaxation towards an exogenous desired velocity.

In a minimal model, the desired velocity, i.e., desired direction (vector) and desired speed (scalar), is assumed exogenous and provided at a tactical modelling level. The microscopic model dynamics for the i -th pedestrian reads

$$\begin{cases} \dot{Q}_{ij}(t) = p_i(t) - p_j(t), & j = 1 \dots, N, j \neq i & Q_{ij}(0) = Q_{ij}^0, \\ \dot{p}_i(t) = \lambda(u_i(t) - p_i(t)) - \sum_{j \neq i} \nabla U(Q_{ij}(t)), & & p_i(0) = p_i^0, \end{cases} \quad (1)$$

with

- exogenous desired velocities

$$u(t) = (u_1(t), \dots, u_N(t)): [0, T] \rightarrow \mathbb{R}^{2 \cdot (N-1)}$$

coming from a tactical model. Even though the desired velocities may be time-dependent in general, they are assumed constant in the following.

- relaxation rate $\lambda \geq 0$ modelling the sensitivity w.r.t. the desired velocity;
- distance-based non-linear repulsive interaction potential given by

$$U : \mathbb{R}^2 \mapsto \mathbb{R}_+, \quad U(x) = AB e^{-|x|/B}, \quad (2)$$

where $|\cdot|$ is the minimal distance on the torus. The potential U is isotropic since it does not depend on the current velocity. The assumption of distance-based repulsion with the neighbors comes from proxemics social concepts and is also safety-motivated as it allows the pedestrians to avoid collisions.

Note that

$$\nabla U(x) = -\frac{x}{|x|} A e^{-|x|/B} = -\nabla U(-x) \quad (3)$$

is an odd function and the implicit assumption that interactions depend only on the distances of two interacting agents. Both will be crucial in the derivation of the PHS formulation later on. Here, we propose to model forces with the help of a gradient of a nonlinear distance-based potential as for example in [43]. In general, any repulsive distance based potential with odd potential can be used. Altogether, the model corresponds to a simplified version of the well-known *social force model* (SFM) by Helbing & Molnár (1995) [35]. The main simplification is that the anisotropic vision field mechanism is neglected. Moreover, we remark that introducing Q_{ij} increases the number of variables. Nevertheless, we note that the information in the system is not altered as the information of each Q_i can be computed knowing one of the other Q_j 's.

2.2. Port-Hamiltonian formulation. It has been shown recently that the Cucker-Smale swarm model can be represented as a port-Hamiltonian system [17]. The formulation is conjectured for large systems and demonstrated with three interacting particles. It turns out that the microscopic model Eq. (1) for N agents can also be formulated as a port-Hamiltonian system. This is the main step towards the formulation of the Hamiltonian-based order parameter which is the main result of this article.

Proposition 1. *Port-Hamiltonian formulation of the microscopic pedestrian system Eq. (1).*

Denoting $Q = (Q_1, \dots, Q_N)$, $p = (p_1, \dots, p_N)$, and $z = (Q, p)^T$, a port-Hamiltonian formulation of the microscopic pedestrian system Eq. (1) is given by

$$\begin{cases} \dot{z}(t) = (J - R)\nabla H(z(t)) + \lambda \tilde{u}(t), & z(0) = (Q^0, p^0), \\ y(z(t)) = \lambda \nabla H(z(t)), \end{cases} \quad (4)$$

with

$$J = \begin{bmatrix} 0 & M \\ -M^T & 0 \end{bmatrix}, \quad R = \begin{bmatrix} 0 & 0 \\ 0 & \lambda I \end{bmatrix}, \quad M = \begin{bmatrix} M_1 \\ \vdots \\ M_N \end{bmatrix}, \quad (5)$$

$$\tilde{u}(t) = [0 \dots 0 \quad u_1(t) \dots u_N(t)]^T, \quad (6)$$

and

$$M_1 = \begin{bmatrix} 1 & -1 & 0 & 0 & \dots & 0 \\ 1 & 0 & -1 & 0 & \dots & 0 \\ \vdots & & & & & \vdots \\ 1 & & & & & -1 \end{bmatrix}, \quad M_2 = \begin{bmatrix} -1 & 1 & 0 & 0 & \dots & 0 \\ 0 & 1 & -1 & 0 & \dots & 0 \\ \vdots & & & & & \vdots \\ 0 & 1 & & & & -1 \end{bmatrix}, \quad \dots \quad (7)$$

Here, $J, R \in \mathbb{R}^{N(N-1) \times N}$, J is skew-symmetric and admits block structure while R is positive semi-definite. The input u allows for control actions and y is the output. The Hamiltonian H is the sum of the distance-based repulsive potentials and quadratic speeds, i.e. the sum of kinetic and potential energy

$$H(z(t)) = \frac{1}{2} \|p(t)\|^2 + \frac{1}{2} \sum_{i=1}^N \sum_{j \neq i}^N U(Q_{ij}(t)). \quad (8)$$

Proof. The port-Hamiltonian formulation Eq. (4) reads

$$\begin{bmatrix} \dot{Q} \\ \dot{p} \end{bmatrix} = \left(\begin{bmatrix} 0 & M \\ -M^T & 0 \end{bmatrix} - \begin{bmatrix} 0 & 0 \\ 0 & \lambda I \end{bmatrix} \right) \begin{bmatrix} \frac{1}{2} \nabla U(Q) \\ p \end{bmatrix} + \lambda \begin{bmatrix} 0 \\ u \end{bmatrix}.$$

The sparse structure of M and the input u yields

$$\dot{Q} = Mp,$$

which implies

$$\dot{Q}_{ij} = p_i - p_j,$$

for each component. The second equality is obtained by observing that

$$\dot{p} = -M^T \frac{1}{2} \nabla U(Q) - \lambda p + \lambda u.$$

This equation reads for every $i = 1, \dots, N$ as

$$\begin{aligned} \dot{p}_i &= \lambda(u_i - p_i) - \frac{1}{2} \sum_{j \neq i} \nabla U(Q_{ij}) - \nabla U(Q_{ji}), \\ &= \lambda(u_i - p_i) - \sum_{j \neq i} \nabla U(Q_{ij}), \end{aligned}$$

where we used $\nabla U(Q_{ji}) = -\nabla U(Q_{ij})$. Altogether, the microscopic model Eq. (1) is recovered. \square

Remark 1. In the port-Hamiltonian formulation, the isotropic structure of the interaction terms is crucial to obtain the skew-symmetric structure of the PHS. Tactical decisions such as desired velocities are regarded as external information and provided through the input-port u . From a physical point of view, the tactical decisions adjust the energy of the system [44]. The parameter λ accounts for the pedestrians’ sensitivity and reactivity to the desired velocity. It appears in both the dissipation matrix and the input control port. The result is a linear input-state-output PHS with dissipation and constant control input. The skew-symmetric part models the motion kinematic by pairwise repulsive social forces. This conservative part of the system yields the pedestrian proxemic and collision-avoidance behaviors. The dissipation matrix together with the input provides external information such as destination or desired speed for each of the pedestrians.

In the presented formulation no interaction ports [2, Eq. (29)] are visible as the interaction ports of the individuals are already coupled in a PHS-preserving manner such that the system of all individual interactions admits a closed PHS structure. Non-linear effects come from the isotropic interaction potential. The absence of boundary ports is because we consider the dynamics on the torus. We illustrate the different components of the port-Hamiltonian pedestrian model in Fig. 2. Here the orange point is the considered pedestrian, while the three blue squares are neighbors. The grey levels in the background quantify the acceleration, the grey level being lighter as the acceleration increases. The plots on the left represent the non-linear isotropic repulsive interaction terms corresponding to the skew-symmetric structure of the PHS. The central plots describe the linear dissipation and control ports, while the plots on the right, summing these two components, represent the resulting acceleration field of the port-Hamiltonian pedestrian model.

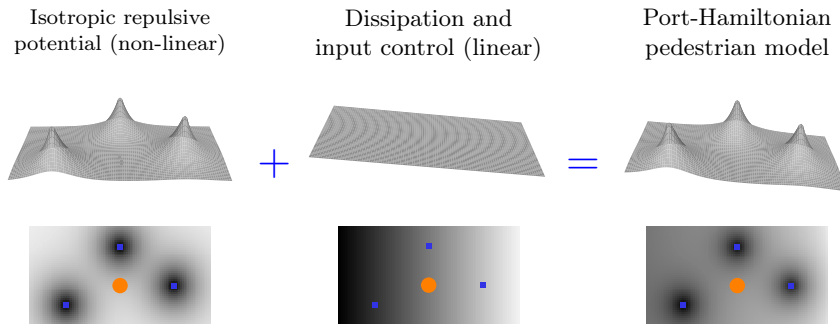


FIGURE 2. Illustrative scheme for the port-Hamiltonian pedestrian model composed of non-linear isotropic repulsive interaction terms corresponding to the skew-symmetric structure of the PHS and linear dissipation and control ports.

Remark 2. Our Hamiltonian formulation is based on isotropic and distance-dependent interactions. In the literature, most force-based pedestrian models include anisotropic repulsion mechanisms to account for fundamental diagrams [45], vision cone effects [35, 46], or preferred crossing directions [43]. The repulsion terms are weighted by factors generally depending on the bearing angle, i.e., the

velocity, breaking the skew-symmetry of the Hamiltonian formulation. In the port-Hamiltonian framework, anisotropic effects can be modelled for example with the help of the state-dependent input terms. Some possible extensions of the PHS model, including anisotropic effects, are discussed in the conclusion.

2.3. Hamiltonian behavior. Exploiting the PHS structure directly we obtain the energy balance

$$\frac{d}{dt}H(z(t)) = y^T(z(t))\tilde{u}(t) - \nabla^T H(z(t)) R \nabla H(z(t)) = \lambda \langle p(t), u(t) - p(t) \rangle. \quad (9)$$

Hence the time derivative of the Hamiltonian depends only on the pedestrians velocities. We observe that the time derivative is zero if all pedestrians move with their desired velocities, i.e.,

$$\frac{d}{dt}H(z(t)) = 0 \quad \text{if} \quad \forall i, p_i(t) = u_i(t). \quad (10)$$

Moreover, the following simple implications hold:

- The Hamiltonian is constant, $\frac{d}{dt}H(z(t)) = 0$ for all $t \geq 0$, if the system has no dissipation, i.e.,

$$\forall t \geq 0, \frac{d}{dt}H(z(t)) = 0 \quad \text{if} \quad \lambda = 0. \quad (11)$$

Indeed, the purely Hamiltonian systems is conservative as expected.

- If $u \equiv 0$, the Hamiltonian decreases over time,

$$\forall t \geq 0, \frac{d}{dt}H(z(t)) \leq 0 \quad \text{if} \quad \forall i, u_i = 0. \quad (12)$$

Dissipation yields asymptotic stability with crystallisation as equilibrium.

- The Hamiltonian is also decreasing if p and u are orthogonal. More generally, the Cauchy-Schwarz inequality provides

$$\langle p(t), u(t) \rangle - \|p(t)\|^2 \leq \|p(t)\| \|u(t)\| - \|p(t)\|^2. \quad (13)$$

Therefore

$$\frac{d}{dt}H(z(t)) \leq \lambda \|p(t)\| (\|u(t)\| - \|p(t)\|) \leq 0, \quad \text{if} \quad \|u(t)\| \leq \|p(t)\|. \quad (14)$$

However, there is no monotone relationship between H and $\|p\|$. The speed may increase even if the Hamiltonian decreases, if, for instance, the distances between the individuals increases. Therefore, having initially $\|u\| \leq \|p^0\|$ is not sufficient to demonstrate that $\frac{d}{dt}H(z(t)) \leq 0$ for all $t \geq 0$.

Remark 3. A final remark concerns the asymptotic behaviour of the Hamiltonian without pedestrian interaction. Assuming the desired velocities u to be constant over time and no interaction takes place, i.e., $A = 0$, the pedestrian velocities simply relax to the desired velocity and the asymptotic behaviour characterized by

$$H(t) \rightarrow H^*(u) := \frac{1}{2} \|u\|^2, \quad \text{as} \quad t \rightarrow \infty. \quad (15)$$

This estimate allows to provide a physical threshold of interaction for the Hamiltonian that lays the ground for the order parameter that will be discussed in detail in Section 3.2.

3. Numerical schemes and simulation results.

3.1. Comparison of numerical schemes. In this section, we test different numerical schemes for the simulation of the particle system. We denote the acceleration of the i -th pedestrian as

$$a(q_i, p_i) = \lambda(u_i - p_i) - \sum_{j \neq i} \nabla U(q_i - q_j). \quad (16)$$

The tested schemes are combinations of explicit (forward) and implicit (backward) Euler methods applied to particle speeds and positions and a truncated version of the leapfrog algorithm.

- Euler explicit/explicit scheme:

$$\begin{cases} p^{k+1} = p^k + \delta t \ a(q^k, p^k) \\ q^{k+1} = q^k + \delta t \ p^k \end{cases} \quad (17)$$

- Euler explicit/implicit scheme:

$$\begin{cases} p^{k+1} = p^k + \delta t \ a(q^k, p^k) \\ q^{k+1} = q^k + \delta t \ p^{k+1} \end{cases} \quad (18)$$

- Euler implicit/explicit scheme:

$$\begin{cases} p^{k+1} = p^k + \delta t \ a(q^{k+1}, p^{k+1}) = p^k + \frac{\delta t}{1 + \lambda \delta t} a(q^{k+1}, p^k) \\ q^{k+1} = q^k + \delta t \ p^k \end{cases} \quad (19)$$

- Euler implicit/implicit scheme:

$$\begin{cases} p^{k+1} = p^k + \delta t \ a(q^{k+1}, p^{k+1}) \\ q^{k+1} = q^k + \delta t \ p^{k+1} \end{cases} \quad (20)$$

Here the equation $p^{k+1} = p^k + \delta t \ a(q^{k+1}, p^{k+1})$ has to be solved numerically.

- Leapfrog scheme:

$$\begin{cases} p^{k+1} = p^k + \frac{\delta t}{2} (a(q^k, p^k) + a(q^{k+1}, p^{k+1})) \\ q^{k+1} = q^k + \delta t \ p^k + \frac{\delta t^2}{2} a(q^k, p^k) \end{cases}$$

Note that

$$a(q^{k+1}, p^{k+1}) = a(q^{k+1}, p^k) + \lambda(p^k - p^{k+1}),$$

and the leapfrog scheme reads after simplification

$$\begin{cases} p^{k+1} = p^k + \frac{\delta t}{2 + \lambda \delta t} (a(q^k, p^k) + a(q^{k+1}, p^k)) \\ q^{k+1} = q^k + \delta t \ p^k + \frac{\delta t^2}{2} a(q^k, p^k) \end{cases} \quad (21)$$

We perform a simulation experiment to compare the precision of the different numerical schemes. We simulate the evolution of 32 particles on an 11 meters \times 5 meters domain with periodic boundary conditions, which can be interpreted as torus. The desired velocity $u = (1, 0)^\top$ is pointing to the right. Initially the particles are randomly distributed on the left part of the domain with zero velocity. Results of an exemplary simulation are presented in Fig. 3. The parameters values are

chosen as in standard models [35, 47], see Table 1 for more details. To quantify whether the port-Hamiltonian dynamics are accurately described, we compare the time derivative of the Hamiltonian provided by the balance equation (9) to the time-difference of the Hamiltonian Eq. (8),

$$\text{Error}_1^k = \lambda \langle p^k, u - p^k \rangle - \frac{1}{\delta t} (H(Q^k, p^k) - H(Q^{k-1}, p^{k-1})). \quad (22)$$

The errors should vanish as $\delta t \rightarrow 0$. We also compute the numerical integral

$$\text{Error}_2^k = \delta t \sum_{i=1}^k \text{Error}_1^i = H(Q^0, p^0) + \lambda \delta t \sum_{i=0}^k \langle p^i, u - p^i \rangle - H(Q^k, p^k), \quad (23)$$

to directly assess the Hamiltonian estimation precision. Such errors, averaged over the first 20 seconds of the simulation, are presented in Fig. 4 for the five schemes and numerical time steps δt ranging from 0.01 to 0.2 s.

Two main characteristics are noteworthy:

- The explicit schemes tend to underestimate the Hamiltonian and its derivative (positive bias) while the implicit schemes overestimate it (negative bias, see Fig. 4, left panels). The leapfrog algorithm error is much more centered and presents almost unbiased estimates.
- In terms of absolute error, the explicit/explicit and explicit/implicit Euler schemes have similar behaviors as do the implicit/explicit Euler and leapfrog schemes (see Fig. 4, right panels); the second pair being much more accurate. The implicit/implicit Euler scheme provides intermediate estimates.

These observations are in accordance with well-known results from ODE theory. Figure 5 presents the scheme efficiency in terms of CPU time. Here, we measure the time required by the different schemes to simulate 20 seconds of the experiment shown in Fig. 3. The three explicit Euler schemes Eqs. (17), (18) and (19) need similar resources. The leapfrog scheme Eq. (21) requires two computations of the acceleration function at each time step and is therefore less effective (by approximately a factor 1.6, see Fig. 5, left panel). Even more computational effort (up to a factor 10) is needed by the implicit Euler scheme Eq. (20) which uses several computations of the acceleration function. On the other hand, the implicit/explicit Euler scheme provides the best approximation in terms of CPU resources for any precision error (see Fig. 5, right panel). Followed by the leapfrog scheme, the other explicit Euler schemes, and, well afterwards, the implicit Euler scheme. Simulation of other scenarios, including counter and crossing flows, showed similar behaviors. Again, the observations coincide with the general theory. The following results are based on the leapfrog discretization.

Parameter	Interpretation	PHS component	Value
λ	Pedestrian sensitivity	Dissipation matrix	2 s^{-1}
$ u $	Desired speed	Input control port	1 m/s
A	Repulsion strength	Skew-symmetric structure	5 ms^{-2}
B	Interaction range	Skew-symmetric structure	0.3 m

TABLE 1. Model parameters and values used for simulation.

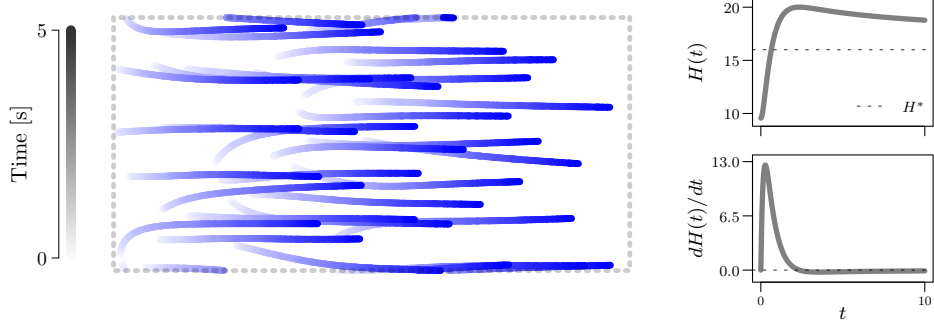


FIGURE 3. Simulation of a uni-direction flow used as a reference to compare the six numerical schemes Eqs. (17)–(21), see Fig. 4. Illustrative example of the leapfrog scheme (21) with $\delta t = 0.001$ s.

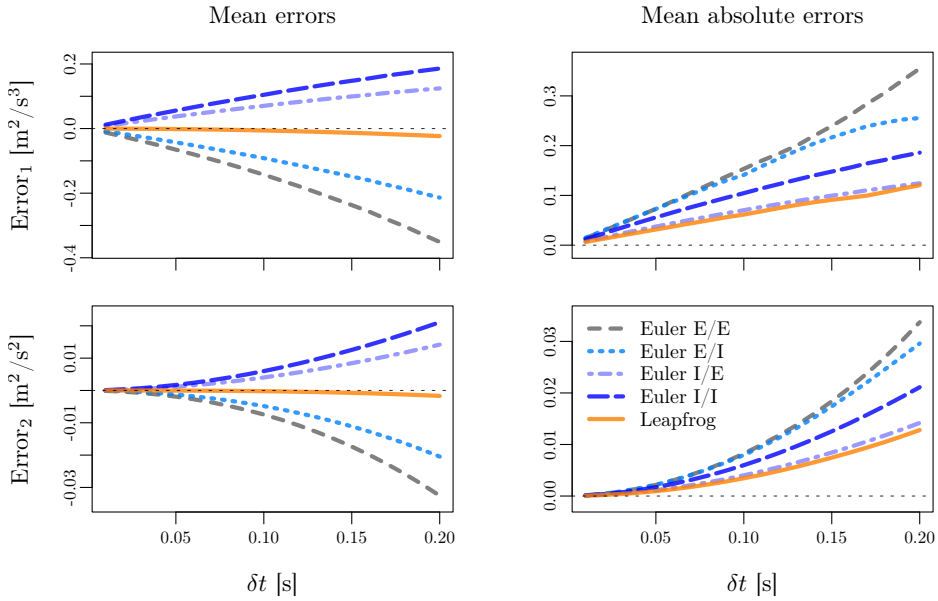


FIGURE 4. Mean numerical errors of the Euler and leapfrog discretisation schemes averaged during the 20 first seconds of the experiment in Fig. 3 for numerical time steps δt ranging from 0.01 to 0.2 s. Top panels: Error resulting from the numerical approximation of the time derivative of the Hamiltonian. Bottom panels: Error resulting from the numerical approximation of the Hamiltonian. The left panels show the mean errors while the right panels show the mean absolute errors. The leapfrog scheme systematically outperforms the implicit and explicit Euler schemes.

3.2. Simulation results. The simulation results presented in the following describe the evolution of 32 particles on an 11 meters \times 5 meters domain with periodic boundary conditions. We consider a mixed flow with opposite desired directions.

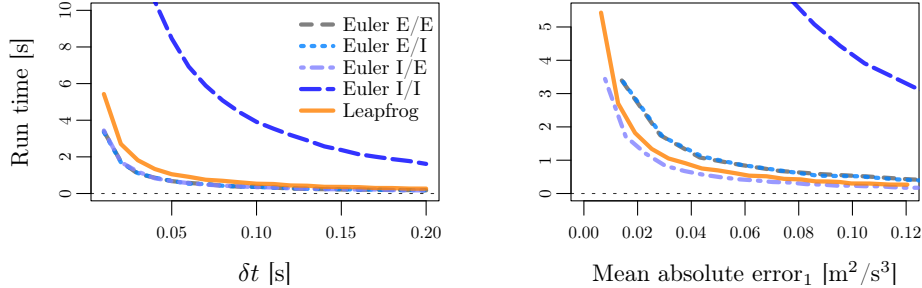


FIGURE 5. Run times of the Euler and leapfrog discretisation schemes for the simulation of the 20 first seconds of experiment in Fig. 3 according to the numerical time step δt (left panel) and the numerical absolute error (right panel). In terms of run time, the explicit Euler schemes are faster than the leapfrog scheme (left panel). In terms of CPU resources, the implicit/explicit Euler scheme provides the best approximation, followed by the leapfrog scheme, the other explicit Euler schemes, and, well afterwards, the implicit Euler scheme (right panel).

The blue particles systematically endeavor to move to the right. The orange particles aim to move to the left for the counter-flow experiment, while the desired direction is to the top for the crossing-flow. The blue and orange particles are initially randomly distributed on the left and right sides of the domain, respectively, in the counter-flow experiment. They are indifferently initially randomly distributed over the domain for the crossing-flow experiment. The initial velocities of all particles are zero for both experiments. The model parameter settings are given in Table 1. All simulations are carried out on NetLogo¹ [48] using the leapfrog scheme (21) with time step $\delta t = 0.001$ s.

3.2.1. *Basic dynamics.* The following simulation results show that the port-Hamiltonian pedestrian model can describe different fundamental dynamics. Let us discuss the basic dynamics:

- Case $\lambda = 0$. No dissipation to the desired velocity occurs if the relaxation rate λ is zero. The system is purely Hamiltonian and the total energy is conserved, see Eq. (11). For A large the system describes disordered dynamics similar to dynamical billiards (2D colloids) governed by the repulsion potential between the particles, see Fig. 6.
- Case $u = 0$. Adding dissipation (i.e., $\lambda > 0$) and neglecting the input control, i.e. $u \equiv 0$ results in crystallization phenomena (see Fig. 7). Indeed, the particles have no preferred direction and the desired velocity is zero. The particles may even reach deterministic hexagonal or squared homogeneous grids according to the interaction distance D if the relaxation λ is sufficiently low. The derivative of the Hamiltonian is nonpositive, see Eq. (12). Hence, the system is dissipative and the Hamiltonian relaxes towards low energy levels.

¹An NetLogo online simulation platform of the port-Hamiltonian pedestrian model is available at https://www.vzu.uni-wuppertal.de/fileadmin/site/vzu/Port-Hamiltonian_pedestrian_model.

- Case $A = 0$. No interactions arise when the interaction potential is zero. The agents relax their speeds to the desired velocity and the Hamiltonian trivially relaxes towards $H^* = Nu^2/2$, see Eq. (15) and Fig. 8.

Dynamics without dissipation ($\lambda = 0$)

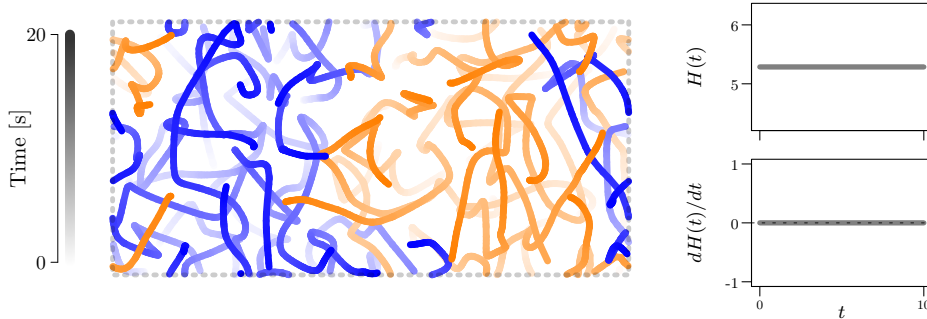


FIGURE 6. Simulation of a counter flow with the port-Hamiltonian pedestrian model for $\lambda = 0$ (pure Hamiltonian case). Leapfrog scheme (21) with $\delta t = 1e-3$ s. The total energy is conserved, the Hamiltonian is constant and the particle dynamics are close to those of a dynamical billiard (2D colloid).

Dynamics with dissipation and without input control ($\lambda > 0, u = 0$)

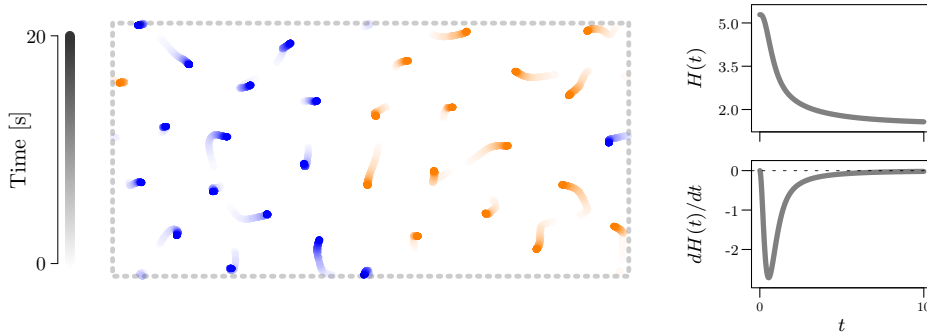


FIGURE 7. Simulation of a counter flow with the port-Hamiltonian pedestrian model for $u = 0$ (dissipative Hamiltonian case). Leapfrog scheme (21) with $\delta t = 1e-3$ s. The energy in the system is progressively dissipated, and the particles crystallise to a homogeneous equilibrium configuration. The Hamiltonian relaxes towards low energy levels.

3.2.2. *Collective dynamics.* The previous studies illustrated the different model components and their roles in the dynamics. However, none of these is realistic for pedestrian dynamics. Force-based models can describe many types of collective dynamics observed in pedestrian crowds, including lane and strip formation for counter and crossing flows, or jamming, arching, and alternating counter flow at bottlenecks [35, 49, 50]. A phase transition occurs from disordered states to coordinated

Dynamics with no pedestrian interaction ($A = 0$)

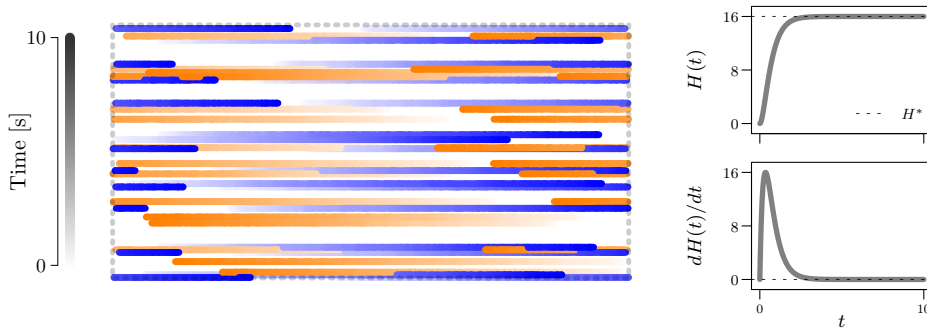


FIGURE 8. Simulation of a counter flow with the port-Hamiltonian pedestrian model for $A = 0$ (no interaction). Leapfrog scheme (21) with $\delta t = 1e-3$ s. The particles relax their velocities towards the desired u while the Hamiltonian converges to $H^* = Nu^2/2 = 16$.

dynamics. Critical parameter settings partition the phase diagram of the system. In the model, lane or strip formation arises for reactive agents, i.e., for λ sufficiently large, while gridlocks occur as the relaxation operates slowly (see Figs. 9 and 10 for counter flow and the lane formation, or Figs. 11 and 12 for counter flow and the strip formation). Numerical tests indicate that the dynamics converge to stable stationary states in case of collective dynamics (i.e., λ large) while they are unstable and seem not to converge for λ small. Indeed, in the port-Hamiltonian framework, the parameter λ balances the dynamics between the skew-symmetric parts enforcing conservation of energy and the dissipation and control input components which vary the energy and lead to long-term stability. Note that other parameters, for instance, the interaction range B , also significantly influence the dynamics. Order parameters are helpful tools to distinguish the different behaviours discussed here. In the following section, we introduce an order parameter that is based on the Hamiltonian. Here, the advantage of the PHS structure of the proposed model become apparent.

4. Hamiltonian as physical order parameter. One challenge in multiscale modelling is the formulation of generic macroscopic order parameters that allow to quantify the system state. Many order parameters have been developed in the literature. In most cases, the order parameters are tailored to detect specific types of collective dynamics. For instance, an order parameter quantifying lane formation reads

$$\Phi_L = \frac{1}{N} \sum_{i=1}^N \phi_i^L \quad (24)$$

with

$$\phi_i^L = \left[\frac{L_i - \underline{L}_i}{L_i + \underline{L}_i} \right]^2 \quad \text{and} \quad \begin{aligned} L_i &= \text{card}(j, |y_i - y_j| < \Delta, u_i = u_j), \\ \underline{L}_i &= \text{card}(j, |y_i - y_j| < \Delta, u_i \neq u_j), \end{aligned}$$

and $(x_i, y_i)_i$ are the positions of the agents and $(u_i)_i$ their desired velocities. Here $\Delta = 0.5$ m, 2Δ being a lane width threshold value. The parameter (24) was initially introduced to detect lanes in a colloidal suspension [51] and used in pedestrian

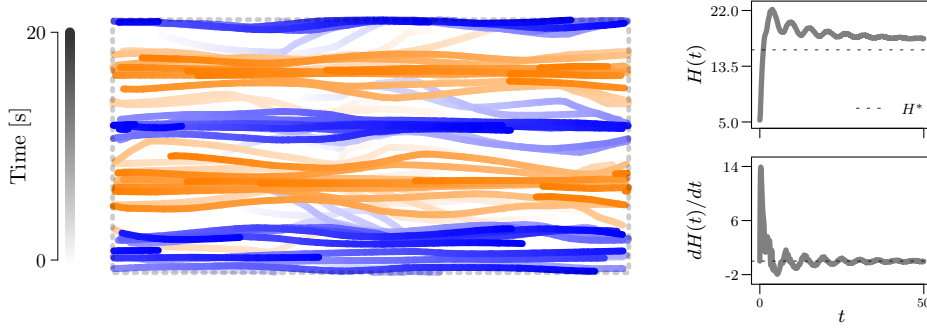
Lane formation for a counter flow ($\lambda = 2 \text{ s}^{-1}$)


FIGURE 9. Simulation of a counter flow with the port-Hamiltonian pedestrian model for $\lambda = 2 \text{ s}^{-1}$ (reactive pedestrian). Leapfrog scheme (21) with $\delta t = 1\text{e-}3 \text{ s}$. Lane formation by motion direction quickly emerges in the dynamics. The Hamiltonian initially fluctuates before stabilising to a value higher than H^* .

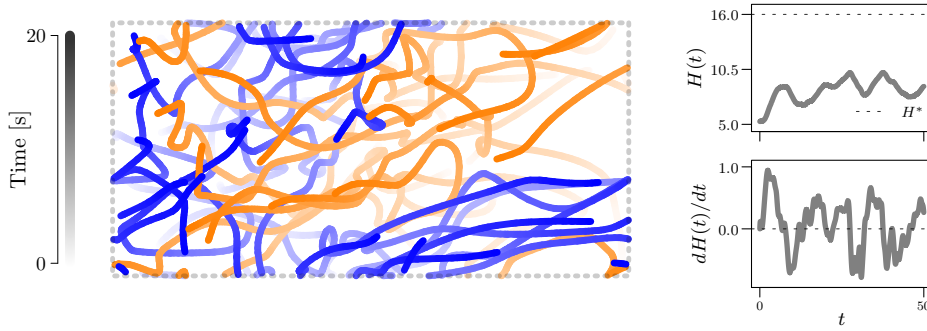
Gridlock for a counter flow ($\lambda = 0.1 \text{ s}^{-1}$)


FIGURE 10. Simulation of a counter flow with the port-Hamiltonian pedestrian model for $\lambda = 0.1 \text{ s}^{-1}$ (low pedestrian reactivity). Leapfrog scheme (21) with $\delta t = 1\text{e-}3 \text{ s}$. No lane formation emerges when the pedestrians are not sufficiently reactive, yielding in gridlocks in the dynamics. The Hamiltonian presents large fluctuations and remains lower than H^* .

dynamics as well [52, 42]. Similarly, an order parameter to detect diagonal strip formation may be formulated as

$$\Phi_S = \frac{1}{N} \sum_{i=1}^N \phi_i^S, \quad (25)$$

with

$$\phi_i^S = \left[\frac{S_i - \underline{S}_i}{S_i + \underline{S}_i} \right]^2 \quad \text{and} \quad \begin{aligned} S_i &= \text{card}(j, |y_i - y_j + x_i - x_j| < \Delta, u_i = u_j), \\ \underline{S}_i &= \text{card}(j, |y_i - y_j + x_i - x_j| < \Delta, u_i \neq u_j). \end{aligned}$$

Strip formation for a crossing flow ($\lambda = 2 \text{ s}^{-1}$)

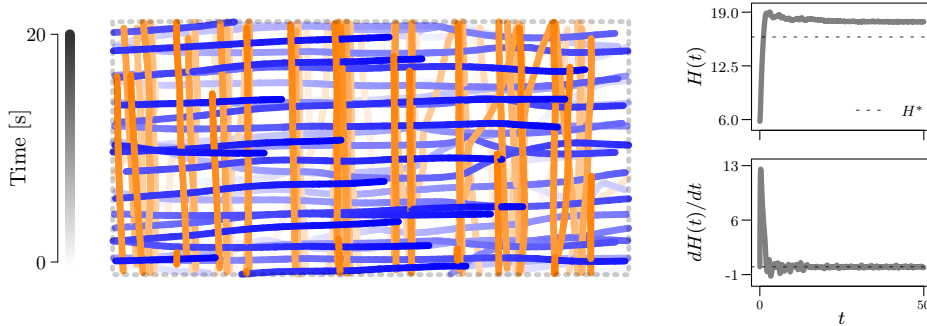


FIGURE 11. Simulation of a counter flow with the port-Hamiltonian pedestrian model for $\lambda = 2 \text{ s}^{-1}$ (reactive pedestrian). Leapfrog scheme (21) with $\delta t = 1\text{e-}3 \text{ s}$. Strip formation diagonal to the motion direction quickly emerges in the dynamics. The configuration for long simulation times is arranged in such a way that pedestrians pass each other without deviating from their desired direction. The Hamiltonian stabilises to a value higher than H^* .

Partial gridlock for a crossing flow ($\lambda = 0.1 \text{ s}^{-1}$)

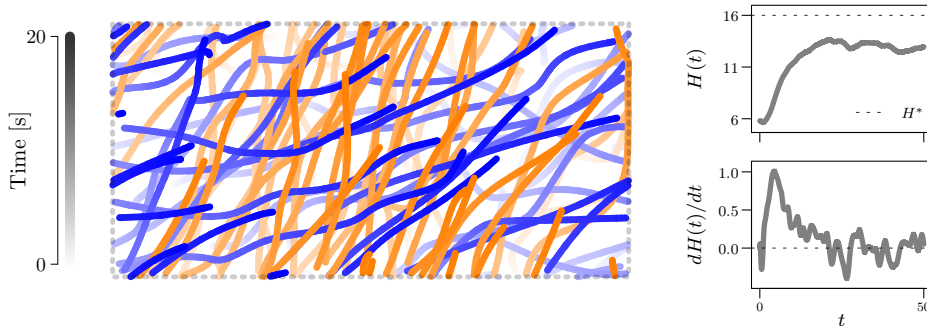


FIGURE 12. Simulation of a counter flow with the port-Hamiltonian pedestrian model for $\lambda = 0.1 \text{ s}^{-1}$ (low pedestrian reactivity). Leapfrog scheme (21) with $\delta t = 1\text{e-}3 \text{ s}$. Strip formation also partly emerges in the dynamics. However, in contrast to the strips obtained for high pedestrian reactivity (see Fig.11), the strips are partly opposed to the desired motion direction, yielding in the formation of diagonal gridlocks deviating the pedestrians. The Hamiltonian remains lower than H^* .

The values of both order parameters, ϕ_i^L and ϕ_i^S , range from zero, when the directions of pedestrians of the same lane or band are uniformly mixed, to one when the pedestrians walk in the same direction.

The Hamiltonian measures the energy in the system. Its value remarkably well quantifies the collective dynamics in the pedestrian port-Hamiltonian model. Indeed, it is systematically high and stable when collective dynamics occur (see Figs. 9 and 11, top right panel), while it is low and fluctuating for disordered states (see

Figs. 10 and 12). The threshold H^* corresponds to the Hamiltonian for agents moving at desired velocities with no interaction, see Eq. (15). We observe that the Hamiltonian is higher than H^* in case of collective behaviors. Indeed, collective dynamics are motions at desired velocity in interaction with neighboring agents. The repulsive interaction potentials lead to values larger than H^* . On the other hand, the Hamiltonian is lower than H^* in case of disordered dynamics with low speed terms and fluctuating distance-based potential terms. Based on these observations we propose an order parameter based on the Hamiltonian given by

$$\Phi_H = \frac{1}{1 + \exp(\kappa(H^* - H))}, \quad \kappa = 100. \quad (26)$$

With this choice we aim to emphasize the difference between the Hamiltonian H and the Hamiltonian value H^* at equilibrium without interaction, see Eq. (15).

A comparison to classical order parameters for lane and strip formation Eqs. (24) and (25), respectively, is shown in Fig. 13. The Hamiltonian order parameter Φ_H polarises in zero and one as $H < H^*$ and $H > H^*$, respectively. The classical and Hamiltonian order parameters are measured for long simulation times with λ ranging from 0.01 to 1 s⁻¹; the dynamics being disordered for low λ (see Figs. 10 and 12) and present lanes or strips for large λ (see Figs. 9 and 11). Interestingly, the critical values for which the classical and Hamiltonian order parameters present a transition coincide for both, counter and crossing flow experiments, see Fig. 13. In contrast to classical order parameters, the Hamiltonian parameter is generic and not tailored for the specific collective dynamics at hand.

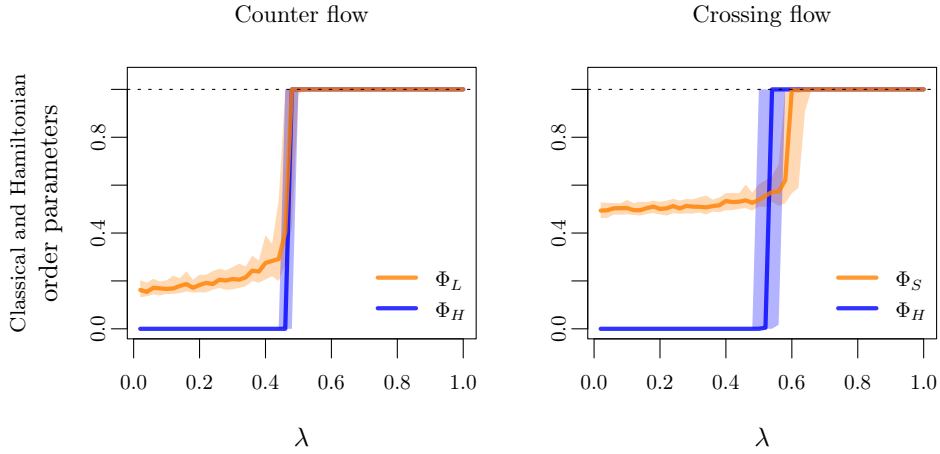


FIGURE 13. Classical order parameters for lane and band formation Eqs. (24) and (25) and Hamiltonian order parameter Eq. (26) for the counter and crossing flow experiments. The curves are median values over 1000 independent simulations while the band are inter-quartile range. Both parameters describe similar phase transitions. Yet, in contrast to classical order parameters, the Hamiltonian parameter is generic and not tailored for the specific collective dynamics at hand.

5. Summary and model development perspectives. In this article, we identify a class of force-based pedestrian models that can be formulated as port-Hamiltonian systems. The general class relies on two main components:

- Isotropic distance-based repulsion between the pedestrians appearing in the skew-symmetric part of the Hamiltonian system.
- Relaxation to the desired velocity provided exogenously from a tactical modelling level which corresponds to dissipation and control.

The resulting PHS is a linear input-state-output port-Hamiltonian system with no interaction port [2]. Non-linear effects come from the isotropic interaction potential. Despite its simplicity, the pedestrian model exhibit many types of collective dynamics of force-based models, e.g., lane formation for counter-flow or strip formation for crossing-flow. Interestingly, the Hamiltonian describes systematic behaviors according to the dynamics, being high and stable in case of collective motion and low and fluctuating in case of disorder. A critical Hamiltonian threshold value relying only on the input control could be identified and physically interpreted. Using the Hamiltonian as a generic macroscopic order parameter in a port-Hamiltonian framework is a natural and promising multiscale modelling approach for pedestrian dynamics. Moreover, there is no need to adapt the order parameter for the specific dynamics at hand.

The Hamiltonian formulation exploits that the pedestrian interactions are assumed to be isotropic and distance-dependent. In the literature, most force-based pedestrian models include anisotropic mechanisms. These mechanisms enable to take vision cone effects [35, 46] or preferred crossing direction [43] into account. The repulsion terms are weighted by factors depending on the bearing angle θ_{ij} or other speed-based factors breaking the symmetry. For instance, in the generalized centrifugal force model [46], the weight is

$$\omega_1(\theta_{ij}) = \begin{cases} \cos(\theta_{ij}) & \text{if } |\theta_{ij}| < \pi/2 \\ 0 & \text{otherwise.} \end{cases} \quad (27)$$

Anisotropic effects also include adaptation of the velocity to the local environment in direction of motion. Such a phenomenological relation between speed and local density is related to the fundamental diagram in traffic engineering. The fundamental diagram is one of the main empirical characteristics of pedestrian dynamics [45, 49]. Altogether, the symmetry of isotropic repulsive interactions is broken by anisotropic effects which we indicate by \times in Fig. 14.

In contrast, the port-Hamiltonian formulation requires the interaction to be odd, hence anisotropic effects need to be incorporated differently. For example, they can result from state-dependent input terms. An extended microscopic model reads in this case

$$\begin{cases} \dot{Q}_{ij}(t) = p_i(t) - p_j(t), & Q_{ij}(0) = Q_{ij}^0, \quad p_i(0) = p_i^0, \\ \dot{p}_i(t) = \lambda(u(t)V(Q_i(t), p_i(t)) - p_i(t)) - \sum_{j \neq i} \nabla U(Q_{ij}(t)), \end{cases} \quad (28)$$

with V a nonlinear optimal velocity function (fundamental diagram) depending on position differences and current velocity. It may also be a function of the velocities of the neighbors to model group effects. The corresponding port-Hamiltonian formulation is

$$\begin{cases} \dot{z}(t) = (J - R)\nabla H(z(t)) + B(z(t))u(t), & z(0) = z_0 \\ y(z(t)) = B^T(z(t))\nabla H(z(t)), \end{cases} \quad (29)$$

with

$$B(z(t)) = \begin{bmatrix} 0 \\ \lambda \operatorname{diag}(V(Q_1(t), p_1(t)), \dots, V(Q_N(t), p_N(t))) \end{bmatrix} \quad (30)$$

a dynamical input matrix. The PHS still admits an input-state-output structure with no interaction port. Yet, nonlinear effects come not only from the interaction potentials but also from the input matrix B operating as a dynamical feedback [44]. The velocity-dependence of V yields an anisotropy and potentially enables to describe fundamental diagrams and other related features such as stop-and-go waves [49]. The challenge (as illustrated in Fig. 14 with the question mark) consists of formulating realistic anisotropic mechanisms through the optimal velocity function V . For instance, the optimal velocity may solely depend on the distance in front [47, 53] or on a preferred crossing side [43]. Other velocity functions may depend on the velocities of the neighbors to model swarming behavior of pedestrian groups.

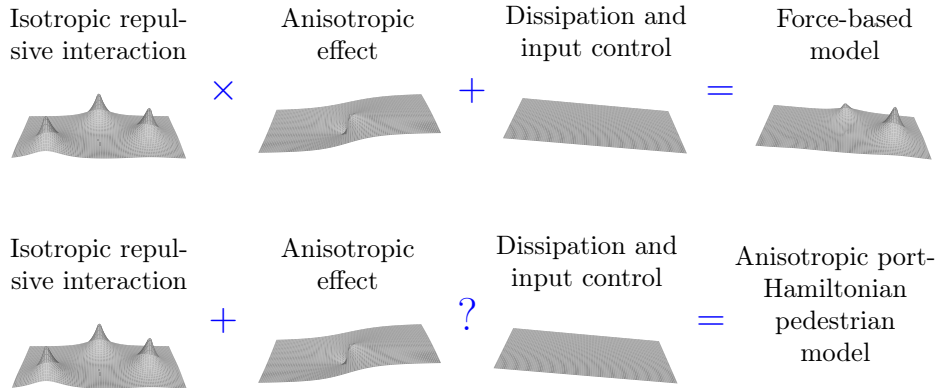


FIGURE 14. Illustrative scheme for possible future development of the port-Hamiltonian pedestrian model incorporating anisotropic effects (e.g., vision field). Top panels: classical force-based framework. Bottom panels: desired port-Hamiltonian formulation.

Acknowledgements. The authors gratefully acknowledge Prof. Andreas Frommer, Prof. Michael Günther, and Dr. Karsten Kahl for meaningful suggestions and support in the formulation and analysis of the numerical schemes. The authors also gratefully acknowledge Prof. Andreas Schadschneider for interesting discussions and relevant remarks regarding the use of the Hamiltonian as order parameter.

Data and results accessibility. An online simulation platform of the port-Hamiltonian pedestrian model on a torus is available at

https://www.vzu.uni-wuppertal.de/fileadmin/site/vzu/Port-Hamiltonian_pedestrian_model.html.

The readers can initiate a simulation and setting $\lambda = 0$, $u = 0$, or $A = 0$ to observe dynamics similar to those presented in Figs. 6, 7 and 8, respectively. The same parameters in combination with scenario *counter-flow* lead to lane formation as in Fig. 9 or to *crossing-flow* for strip formation as in Fig. 11. The gridlocks shown in Figs. 10 and 12 are obtained for small λ .

REFERENCES

- [1] Google Scholar. Accessed: 2022-07-17.
- [2] Arjan van der Schaft. Port-hamiltonian systems: an introductory survey. In *Proceedings of the international congress of mathematicians*, volume 3, pages 1339–1365. Citeseer, 2006.
- [3] Arjan van der Schaft and Dimitri Jeltsema. Port-hamiltonian systems theory: An introductory overview. *Foundations and Trends in Systems and Control*, 1(2-3):173–378, 2014.
- [4] Arjan van der Schaft. Symmetries and conservation laws for hamiltonian systems with inputs and outputs: A generalization of noether’s theorem. *Systems & Control Letters*, 1(2), 1981.
- [5] An intrinsic hamiltonian formulation of network dynamics: Non-standard poisson structures and gyrators. *Journal of the Franklin institute*, 329(5):923–966, 1992.
- [6] Bernhard Maschke and Arjan van der Schaft. Port-controlled hamiltonian systems: modelling origins and systemtheoretic properties. In *Nonlinear Control Systems Design 1992*, pages 359–365. Elsevier, 1993.
- [7] Arjan van der Schaft. Port-hamiltonian systems: network modeling and control of nonlinear physical systems. In *Advanced dynamics and control of structures and machines*, pages 127–167. Springer, 2004.
- [8] Arjan van der Schaft and Bernhard Maschke. Port-hamiltonian systems on graphs. *SIAM Journal on Control and Optimization*, 51(2):906–937, 2013.
- [9] Ramy Rashad, Federico Califano, Arjan van der Schaft, and Stefano Stramigioli. Twenty years of distributed port-hamiltonian systems: a literature review. *IMA Journal of Mathematical Control and Information*, 37(4):1400–1422, 2020.
- [10] Steffi Knorn, Zhiyong Chen, and Richard H Middleton. Overview: Collective control of multi-agent systems. *IEEE Transactions on Control of Network Systems*, 3(4):334–347, 2015.
- [11] Steffi Knorn and Anders Ahlén. Deviation bounds in multi agent systems described by undirected graphs. *Automatica*, 67:205–210, 2016.
- [12] Bing Wang, Xinghu Wang, and Honghua Wang. Output synchronization of multi-agent port-hamiltonian systems with link dynamics. *Kybernetika*, 52(1):89–105, 2016.
- [13] Andrea Cristofaro, Gaetano Giunta, and Paolo Robuffo Giordano. Fault-tolerant formation control of passive multi-agent systems using energy tanks. *IEEE Control Systems Letters*, 2022.
- [14] Arjan van der Schaft and Bernhard Maschke. Port-hamiltonian dynamics on graphs: Consensus and coordination control algorithms. *IFAC Proceedings Volumes*, 43(19):175–178, 2010.
- [15] Dong Xue, Sandra Hirche, and Ming Cao. Opinion behavior analysis in social networks under the influence of cooperative media. *IEEE Transactions on Network Science and Engineering*, 7(3):961–974, 2019.
- [16] Miel Sharf and Daniel Zelazo. Analysis and synthesis of mimo multi-agent systems using network optimization. *IEEE Transactions on Automatic Control*, 64(11):4512–4524, 2019.
- [17] Ion Matei, Christos Mavridis, John S Baras, and Maksym Zhenirovskyy. Inferring particle interaction physical models and their dynamical properties. In *2019 IEEE 58th Conference on Decision and Control (CDC)*, pages 4615–4621. IEEE, 2019.
- [18] Yan Ma, Jian Chen, Junmin Wang, Yanchuan Xu, and Yuexuan Wang. Path-tracking considering yaw stability with passivity-based control for autonomous vehicles. *IEEE Transactions on Intelligent Transportation Systems*, 2021.
- [19] Steffi Knorn, Alejandro Donaire, Juan C Agüero, and Richard H Middleton. Passivity-based control for multi-vehicle systems subject to string constraints. *Automatica*, 50(12):3224–3230, 2014.
- [20] Siyuan Dai and Xenofon Koutsoukos. Safety analysis of integrated adaptive cruise control and lane keeping control using discrete-time models of port-hamiltonian systems. In *2017 American Control Conference (ACC)*, pages 2980–2985. IEEE, 2017.
- [21] Siyuan Dai and Xenofon Koutsoukos. Safety analysis of integrated adaptive cruise and lane keeping control using multi-modal port-hamiltonian systems. *Nonlinear Analysis: Hybrid Systems*, 35:100816, 2020.
- [22] Harshit Bansal, P Schulze, Mohammad Hossein Abbasi, Hans Zwart, Laura Iapichino, Wil HA Schilders, and Nathan van de Wouw. Port-hamiltonian formulation of two-phase flow models. *Systems & Control Letters*, 149:104881, 2021.
- [23] Ramy Rashad, Federico Califano, Frederic P Schuller, and Stefano Stramigioli. Port-hamiltonian modeling of ideal fluid flow: Part i. foundations and kinetic energy. *Journal of geometry and physics*, 164:104201, 2021.

- [24] Kazumasa Hirai and K Tarui. A simulation of the behavior of a crowd in panic. In *Proceedings of the 1975 International Conference on Cybernetics and Society*, pages 409–411, 1975.
- [25] L. F. Henderson. The statistics of crowd fluids. *Nature*, 229:381–383, 1971.
- [26] Francisco Martinez-Gil, Miguel Lozano, Ignacio Garcia-Fernández, and Fernando Fernández. Modeling, evaluation, and scale on artificial pedestrians: a literature review. *ACM Computing Surveys (CSUR)*, 50(5):1–35, 2017.
- [27] Mohcine Chraïbi, Antoine Tordeux, Andreas Schadschneider, and Armin Seyfried. *Modelling of Pedestrian and Evacuation Dynamics*, pages 1–22. Springer Berlin Heidelberg, Berlin, Heidelberg, 2018.
- [28] Nicola Bellomo and Christian Dogbe. On the modeling of traffic and crowds: A survey of models, speculations, and perspectives. *SIAM review*, 53(3):409–463, 2011.
- [29] Giacomo Albi, Nicola Bellomo, Luisa Fermo, S-Y Ha, J Kim, Lorenzo Pareschi, David Poyato, and Juan Soler. Vehicular traffic, crowds, and swarms: From kinetic theory and multiscale methods to applications and research perspectives. *Mathematical Models and Methods in Applied Sciences*, 29(10):1901–2005, 2019.
- [30] Nicola Bellomo, Livio Gibelli, Annalisa Quaini, and Alessandro Reali. Towards a mathematical theory of behavioral human crowds. *Mathematical Models and Methods in Applied Sciences*, pages 1–38, 2022.
- [31] Michael Fischer, Gaspard Jankowiak, and Marie-Therese Wolfram. Micro- and macroscopic modeling of crowding and pushing in corridors. *Networks and Heterogeneous Media*, 15(3):405–426, 2020.
- [32] Julien Barré, Pierre Degond, Diane Peurichard, and Ewelina Zatorska. Modelling pattern formation through differential repulsion. *Networks and Heterogeneous Media*, 15(3):307–352, 2020.
- [33] Martin Burger, Lisa Maria Kreusser, and Claudia Totzeck. Mean-field optimal control for biological pattern formation. *ESAIM: Control, Optimisation and Calculus of Variations*, 27:40, 2021.
- [34] Martin Burger, René Pinnau, Claudia Totzeck, and Oliver Tse. Mean-field optimal control and optimality conditions in the space of probability measures. *SIAM Journal on Control and Optimization*, 59(2):977–1006, 2021.
- [35] Dirk Helbing and Peter Molnár. Social force model for pedestrian dynamics. *Phys. Rev. E*, 51(5):4282–4286, 1995.
- [36] Mohcine Chraïbi, Ulrich Kemloh, Andreas Schadschneider, and Armin Seyfried. Force-based models of pedestrian dynamics. *Networks & Heterogeneous Media*, 6(3):425, 2011.
- [37] Jur Van den Berg, Ming Lin, and Dinesh Manocha. Reciprocal velocity obstacles for real-time multi-agent navigation. In *2008 IEEE International Conference on Robotics and Automation*, pages 1928–1935. IEEE, 2008.
- [38] Jurg van den Berg, Stephen Guy, Ming Lin, and Dinesh Manocha. Reciprocal n-body collision avoidance. In *Robotics Research: The 14th International Symposium ISRR*, pages 3–19, Berlin, Heidelberg, 2011. Springer.
- [39] Wouter Van Toll and Julien Pettré. Algorithms for microscopic crowd simulation: Advances in the 2010s. In *Computer Graphics Forum*, volume 40, pages 731–754. Wiley Online Library, 2021.
- [40] Mohcine Chraïbi, Takahiro Ezaki, Antoine Tordeux, Katsuhiko Nishinari, Andreas Schadschneider, and Armin Seyfried. Jamming transitions in force-based models for pedestrian dynamics. *Physical Review E*, 92(4):042809, 2015.
- [41] Stefan Nowak and Andreas Schadschneider. Quantitative analysis of pedestrian counterflow in a cellular automaton model. *Physical review E*, 85(6):066128, 2012.
- [42] Basma Khelfa, Raphael Korbmacher, Andreas Schadschneider, and Antoine Tordeux. Heterogeneity-induced lane and band formation in self-driven particle systems. *Scientific reports*, 12(1):1–11, 2022.
- [43] Claudia Totzeck. An anisotropic interaction model with collision avoidance. *Kinetic and Related Models*, 13(6):1219–1242, 2020.
- [44] Romeo Ortega, Arjan Van Der Schaft, Iven Mareels, and Bernhard Maschke. Putting energy back in control. *IEEE Control Systems Magazine*, 21(2):18–33, 2001.
- [45] Armin Seyfried, Bernhard Steffen, Wolfram Klingsch, and Maik Boltes. The fundamental diagram of pedestrian movement revisited. *Journal of Statistical Mechanics: Theory and Experiment*, 2005(10):P10002, 2005.

- [46] Mohcine Chraibi, Armin Seyfried, and Andreas Schadschneider. Generalized centrifugal-force model for pedestrian dynamics. *Physical Review E*, 82(4):046111, 2010.
- [47] Antoine Tordeux, Mohcine Chraibi, and Armin Seyfried. Collision-free speed model for pedestrian dynamics. In *Traffic and Granular Flow'15*, pages 225–232. Springer, 2016.
- [48] Uri Wilensky. Netlogo. evanston, il: Center for connected learning and computer-based modeling, northwestern university, 1999.
- [49] Maik Boltes, Jun Zhang, Antoine Tordeux, Andreas Schadschneider, and Armin Seyfried. *Empirical Results of Pedestrian and Evacuation Dynamics*, pages 1–29. Springer, Berlin, Heidelberg, 2018.
- [50] Andreas Schadschneider, Mohcine Chraibi, Armin Seyfried, Antoine Tordeux, and Jun Zhan. *Pedestrian Dynamics - From Empirical Results to Modeling*, pages 63–102. Birkhäuser, Cham, 2018.
- [51] Martin Rex and Hartmut Löwen. Lane formation in oppositely charged colloids driven by an electric field: Chaining and two-dimensional crystallization. *Phys. Rev. E*, 75:051402, 2007.
- [52] Stefan Nowak and Andreas Schadschneider. Quantitative analysis of pedestrian counterflow in a cellular automaton model. *Phys. Rev. E*, 85:066128, 2012.
- [53] Qiancheng Xu, Mohcine Chraibi, Antoine Tordeux, and Jun Zhang. Generalized collision-free velocity model for pedestrian dynamics. *Physica A: Statistical Mechanics and its Applications*, 535:122521, 2019.

E-mail address: tordeux@uni-wuppertal.de

E-mail address: totzeck@uni-wuppertal.de